

Complex classical motion in potentials with poles and turning points

Carl M. Bender^{a*} and Daniel W. Hook^{a,b†}

^a*Physics Department, Washington University, St. Louis, MO 63130, USA and*

^b*Theoretical Physics, Imperial College, London SW7 2AZ, UK*

(Dated: February 18, 2014)

Complex trajectories for Hamiltonians of the form $H = p^n + V(x)$ are studied. For $n = 2$ time-reversal symmetry prevents trajectories from crossing. However, for $n > 2$ trajectories may indeed cross, and as a result, the complex trajectories for such Hamiltonians have a rich and elaborate structure. In past work on complex classical trajectories it has been observed that turning points act as attractors; they pull on complex trajectories and make them veer towards the turning point. In this paper it is shown that the poles of $V(x)$ have the opposite effect — they deflect and repel trajectories. Moreover, poles shield and screen the effect of turning points.

PACS numbers: 11.30.Er, 02.30.Fn, 05.45.-a

I. INTRODUCTION

A \mathcal{PT} -symmetric quantum system is typically governed by a complex Hamiltonian. Moreover, the boundary conditions on the Schrödinger eigenvalue problem associated with a \mathcal{PT} -symmetric Hamiltonian are imposed in the complex plane. Thus, when one examines the classical limit of a \mathcal{PT} -symmetric system, one is led inevitably to the study of complex classical dynamics. A complex classical dynamical system having one complex degree of freedom is governed by a Hamiltonian of the form $H(x, p)$, where H is often assumed to be analytic in both x and p except for isolated singularities or branch cuts in x . For such a system, Hamilton's equations read

$$\dot{x} = \frac{\partial H}{\partial p}, \quad \dot{p} = -\frac{\partial H}{\partial x}. \quad (1)$$

In this paper we use both analytical and numerical techniques to examine the solutions to these differential equations for complex $x(t)$ and $p(t)$. To do this we decompose $x(t)$ and $p(t)$ into their real and imaginary parts,

$$\begin{aligned} x(t) &= \text{Re } x(t) + i \text{Im } x(t), \\ p(t) &= \text{Re } p(t) + i \text{Im } p(t), \end{aligned} \quad (2)$$

and solve the resulting coupled system of ordinary differential equations. Complex dynamical systems are interesting in part because the particle trajectories $x(t)$ typically lie on multisheeted Riemann surfaces. We explore the qualitative features of the classical particle trajectories in the complex- x plane, and in particular, we compare the behavior of trajectories in the vicinity of turning points and in the vicinity of poles of H . The principal result in this paper is that turning points act as attractors (trajectories are drawn to and pulled around turning

points), but poles tend to repel trajectories and can even screen the effects of turning points.

While complex classical mechanics is a relatively new field there have already been many papers published on the properties of complex phase space [1–26]. Most of these studies have focused on Hamiltonians of the form $H(x, p) = p^2 + V(x)$. For such Hamiltonians the complex trajectories associated with a given energy E cannot intersect. This is because the Hamiltonian is invariant under classical time reversal $t \rightarrow -t$. For a given value of x there are two possible values of the complex velocity \dot{x} , one corresponding to the trajectory going forward in time and the other corresponding to the trajectory going backward in time. However, Hamiltonians such as

$$H(x, p) = p^n + V(x) \quad (n > 2) \quad (3)$$

can have trajectories that cross themselves. For a given value of E there may be n trajectories emanating from a point x , each one having a different complex value of \dot{x} . Furthermore, if n is odd, H is not time-reversal invariant. This means that if we allow time to run backward, a trajectory will not retrace itself. Hamiltonians of the form (3) are especially interesting because, as was shown in Ref. [11], the turning points of these Hamiltonians deflect nearby trajectories by an angle that depends on n ; $n = 2$ gives a deflection of 180° , $n = 3$ gives a deflection of 240° , $n = 4$ gives a deflection of 270° , and so on.

Figure 1 illustrates some of the features of the complex classical trajectories discussed in this paper. This figure shows nine trajectories associated with the Hamiltonian

$$H = p^3 + \frac{x}{1+x^2}. \quad (4)$$

For each of these trajectories the classical energy is $E = \frac{1}{3}$. The nine trajectories emanate from three points in the complex- x plane, $-1 + i$, $1 - i$, and $2 + 2i$. There are two simple poles located at $x = \pm i$ and two turning points on the real axis located at $x = \frac{1}{2}(3 \pm \sqrt{5})$. The trajectories enclosing the turning points rotate through an angle of 240° . Note that the trajectory emanating

*Electronic address: cmb@wustl.edu

†Electronic address: d.hook@imperial.ac.uk

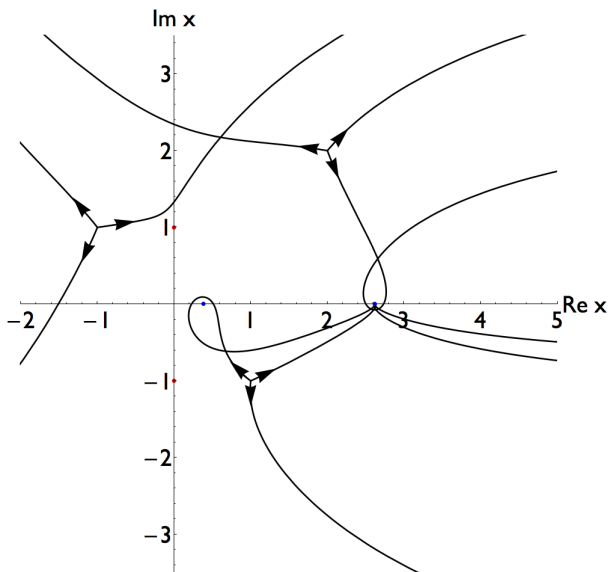


FIG. 1: Nine complex trajectories associated with the Hamiltonian (4). All trajectories represent the complex motion of particles having energy $E = \frac{1}{3}$. There are two turning points at $x = \frac{1}{2}(3 \pm \sqrt{5})$ (blue dots in electronic version) and two poles at $x = \pm i$ (red dots). Because the Hamiltonian contains a cubic momentum term, at each point in the complex- x plane there are three possible directions for the classical trajectories, and these directions are separated by 120° . We have chosen three points at random, $-1 + i$, $1 - i$, and $2 + 2i$, and have plotted the three trajectories originating from each point. The trajectory that begins at $1 - i$ in the northwest direction encircles both turning points and is deflected by 240° each time. Note that the path does not intersect itself because it crosses branch cuts emanating from the turning points and lies on different sheets of a Riemann surface. The trajectory that begins at $-1 + i$ in an eastward direction is pushed to the north by the simple pole at $x = i$; consequently, the trajectory is only slightly affected by the turning points.

from $x = -1 + i$ and going eastward is deflected upward by the pole at $x = i$.

In earlier studies of complex classical mechanical systems many interesting features were discovered. For example, in Ref. [13] it was shown that a complex classical particle can effectively *tunnel* through a potential barrier on the real axis by following a trajectory in the complex plane that goes around the barrier. It was also shown that classical mechanics could mimic quantum tunneling if the energy had a small imaginary part. This idea was further developed in Ref. [22]. Most recently, Turok showed that these complex classical trajectories contribute to the saddle point of the functional integral that represents the tunneling amplitude [26].

To illustrate the advantage of complex classical mechanics, we use complex classical trajectories to explain intuitively how an upside-down \mathcal{PT} -symmetric potential in quantum mechanics can possess discrete positive-energy bound states. The Hamiltonian for a quartic os-

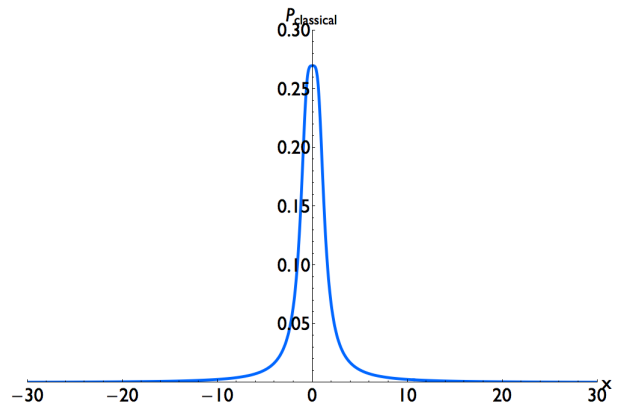


FIG. 2: Classical probability as shown in (7) for $-30 \leq x \leq 30$. Here, the classical energy is $E = 1$.

cillator with an upside-down quartic potential is

$$H = p^2 - x^4. \quad (5)$$

The quantum energy levels of this \mathcal{PT} -symmetric Hamiltonian are known rigorously to be real, positive, and discrete [27–31]. The quantum-mechanical treatment of this system requires that the boundary conditions on the time-independent Schrödinger equation be imposed in Stokes wedges in the complex plane. To understand the quantum theory heuristically we examine the classical equations of motion (1) for this Hamiltonian:

$$\dot{x} = 2p, \quad \dot{p} = 4x^3. \quad (6)$$

For a particle of energy E , the classical velocity is $\dot{x} = 2\sqrt{E + x^4}$. A classical particle is most likely to be found where it is going slowest. Thus, for real x the *normalized classical probability density* $P_{\text{classical}}$, which is the inverse of the particle velocity, is

$$P_{\text{classical}}(x) = \frac{2E^{1/4}\sqrt{\pi}}{\Gamma^2(1/4)\sqrt{E + x^4}}. \quad (7)$$

This probability function for $E = 1$ is plotted in Fig. 2 for real x . Note that the probability density is sharply peaked at $x = 0$, which indicates that the classical particle is most likely to be found near the origin. (It spends most of its time there.) Thus, we see indications that the quantum particle may be in a localized bound state.

The key to understanding how an upside-down potential confines quantum particles relies on calculating the time for a classical particle of energy E to travel to infinity. The time of flight T from $x = 0$ to $x = \infty$ is

$$T = \int_{t=0}^T dt = \int_{x=0}^{\infty} \frac{dx}{\dot{x}}, \quad (8)$$

which is *finite*. One may then ask, If the particle reaches infinity in finite time, where does the particle go next? To answer this question we investigate the particle motion in

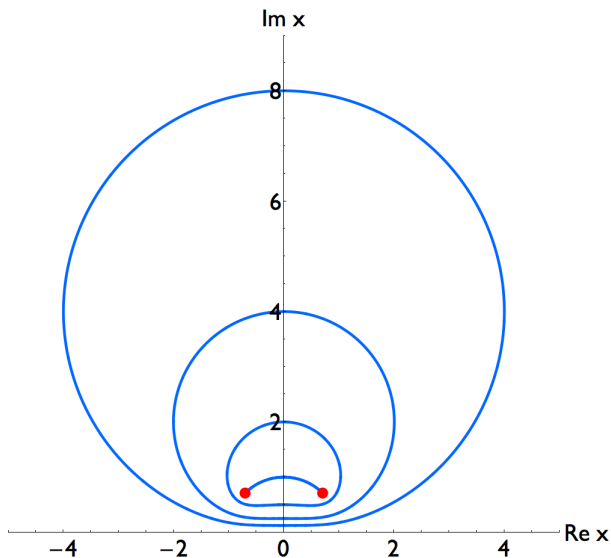


FIG. 3: Closed periodic trajectories in the upper-half x -plane. The energy is $E = 1$. Turning points are located at $x = e^{i\pi/4}$ and $x = e^{3i\pi/4}$ and are indicated by dots. (The two turning points in the lower-half plane are not shown.) Initial conditions are $x_0 = i, \frac{i}{2}, \frac{i}{4}, \frac{i}{8}$.

the complex- x plane. Four trajectories in the upper-half x -plane are shown in Fig. 3. Note that the trajectories are all *closed* and *periodic*. (One of the trajectories is an oscillatory motion between the turning points at $x = e^{i\pi/4}$ and $x = e^{3i\pi/4}$.)

Observe that as the trajectories in Fig. 3 approach the real axis, the classical particle does not simply disappear at $x = \infty$. Rather, as the classical particle reaches $x = +\infty$, it instantly reappears at $x = -\infty$. Thus, the classical particle *periodically* completes the transit from $-\infty$ to $+\infty$. (This periodic motion is equivalent to having a source of particles at $-\infty$ and a sink of particles at $+\infty$.) A three-dimensional plot of the absolute value of the complex classical probability is shown in Fig. 4.

To understand why the corresponding quantum energy is discrete rather than continuous, recall the Bohr-Sommerfeld concept of quantization. We argue that a quantum particle is a wave, and if the classical motion is periodic, the wave must interfere with itself constructively. The condition for constructive interference is

$$\oint dx \sqrt{E - V(x)} = (n + \frac{1}{2}) \pi, \quad (9)$$

which is the complex version of the WKB quantization condition. Thus, complex classical mechanics provides the insight to explain how complex quantum mechanical systems work.

This paper is organized as follows. Section II explains and illustrates the nature of complex classical turning points and poles. Then, Sec. III examines several examples of Hamiltonians of the form $H = p^2 + V(x)$, where

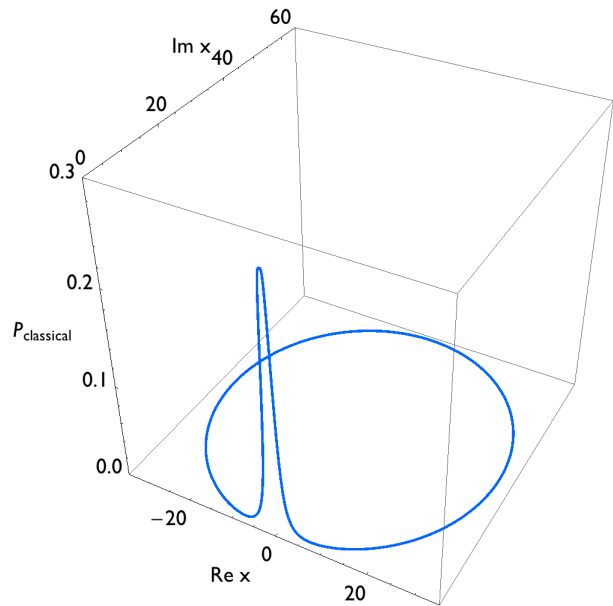


FIG. 4: Three-dimensional plot of the probability (inverse of the absolute value of \dot{x}) for a contour beginning at $x_0 = \frac{i}{64}$ in the complex plane. The classical energy is $E = 1$. The classical particle executes a rapid loop in the complex plane but slows down near the origin. Note that the shape of the peak is the same as that in Fig. 2.

the potential $V(x)$ has poles of order 1, 2, or 3. In Sec. IV we study some Hamiltonians of the form in (3). Finally, in Sec. V we make some brief concluding remarks.

II. ELEMENTARY ILLUSTRATIONS OF THE EFFECTS OF POLES AND TURNING POINTS

In this section we demonstrate the effects of poles and turning points on complex classical trajectories by using simple Hamiltonians of the form

$$H = p^2 \pm x^{-n} \quad (n = 1, 2, 3). \quad (10)$$

To our knowledge, complex classical trajectories for such potentials have not been studied before. (In Ref. [17] complex elliptic potentials with double poles were considered, but the emphasis was on deterministic random walks in a doubly-periodic complex grid and not on the behavior of trajectories near poles.) For the Hamiltonians (10) there is one pole of order n at the origin and n turning points in the complex- x plane. In Figs. 5–7, we plot complex trajectories for the cases $n = 1, 2$, and 3. The left (right) panel of each figure corresponds to the positive (negative) sign in H . In all cases we can see that turning points attract trajectories and cause the trajectories to be deflected. However, the poles repel trajectories and tend to screen out the effects of the turning points. To understand the dynamics, we note that a classical particle goes slowly in the vicinity of a turning point,

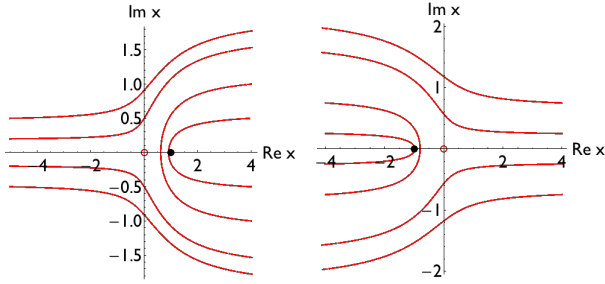


FIG. 5: Complex classical trajectories for the Hamiltonian (10) with $n = 1$. The potential is $1/x$ (left panel) and $-1/x$ (right panel). The energy is $E = 1$. There is one turning point at $x = 1$ (left panel) and $x = -1$ (right panel). Turning points are designated by filled dots. In both panels the pole at the origin is indicated by a hollow circle. Left panel: trajectories begin at $4 - \frac{i}{2}$, $4 - i$, $-5 + \frac{i}{2}$, $-5 + \frac{i}{5}$, $-5 - \frac{i}{5}$, $-5 - \frac{i}{2}$. Right panel: trajectories begin at $-4 + \frac{3i}{4}$, $-4 + \frac{i}{4}$, $4 + \frac{3i}{4}$, $4 + \frac{i}{4}$, $4 - \frac{i}{4}$, $4 - \frac{3i}{4}$. In all cases the turning points attract and deflect trajectories while the poles repel them.

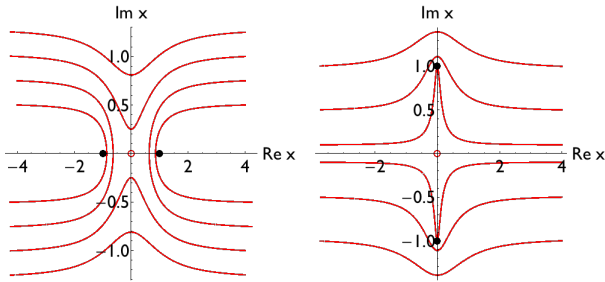


FIG. 6: Here, the potential is x^{-2} for the left panel and $-x^{-2}$ for the right panel. For both panels the energy is $E = 1$, so there are two turning points (indicated by filled circles). In both panels the double pole at the origin is indicated by a hollow circle. Left panel: trajectories begin at $4 + \frac{3i}{4}$, $4 + \frac{i}{2}$, $-4 + \frac{3i}{4}$, $-4 + \frac{i}{2}$, $4 + \frac{5i}{4}$, $5 + i$, $4 - i$, $4 - \frac{5i}{4}$. Right panel: trajectories begin at $4 + i$, $4 + \frac{i}{2}$, $4 + \frac{i}{10}$, $4 - \frac{i}{10}$, $4 - \frac{i}{2}$, $4 - i$. All trajectories in the right panel are deflected around one of the two turning points, while in the left panel the pole overpowers the influence of the turning points on four of the trajectories.

and hence the turning point can have a strong long-range effect on the trajectory. However, if a pole lies between the trajectory and the turning point, the turning point has little or no effect.

III. POTENTIALS WITH TWO SIMPLE POLES

We have examined in greater detail two potentials, $V_1(x)$ and $V_2(x)$, each having two simple poles:

$$V_1(x) = \frac{x}{x^2 + 1}, \quad V_2(x) = \frac{ix}{x^2 + 1}. \quad (11)$$

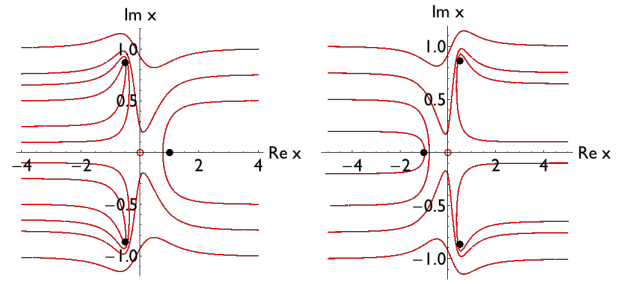


FIG. 7: Here, the potential is $\pm x^{-3}$ and the energy is $E = 1$, so there are three turning points at $x = 1$, $x = e^{\pm 2\pi i/3}$ in the left panel and at $x = -1$ and $x = -1e^{\pm 2\pi i/3}$ in the right panel. A third-order pole lies at the origin in both panels. Trajectories in the left panel begin at $-4 + \frac{i}{2}$, $-4 + \frac{i}{10}$, $-4 - \frac{i}{10}$, $-4 - \frac{i}{2}$, $4 - \frac{i}{2}$, $4 + i$, $4 + \frac{3i}{4}$, $4 - \frac{3i}{4}$, $4 - i$. Trajectories in the right panel begin at $-5 + \frac{i}{2}$, $-5 + \frac{i}{5}$, $5 + \frac{i}{10}$, $5 - \frac{i}{10}$, $-5 + i$, $-5 + \frac{3i}{4}$, $-5 - i\frac{3i}{4}$, $-5 - i$.

In the two subsections that follow we describe the behavior of trajectories in proximity to separatrices and we study Zeno-type behavior (trajectories that approach turning points as $t \rightarrow \infty$).

A. Separatrix and Zeno behavior for $V_1(x)$

If we choose the energy to be $E = \frac{1}{2}$ for the Hamiltonian $H = p^2 + V_1(x)$, there is just one turning point at $x = 1$, which is a *double* turning point; that is, a coalescence of two simple turning points as E approaches $\frac{1}{2}$. There are two poles at $\pm i$. Figure 8 illustrates a bifurcation and a complex Zeno effect. We observe the following: The solid curves in the figure are separatrices. If a trajectory begins between the upper and lower solid curves (red and blue in the electronic version), it approaches the double turning point at $x = 1$ on the real axis as $t \rightarrow \infty$. However, trajectories that begin above the upper separatrix or below the lower separatrix are repelled by the poles at $\pm i$, move off to $\text{Re } x = \pm\infty$ as $t \rightarrow \infty$, and are never captured by the turning point. The two separatrix curves that connect the poles to the turning point distinguish between trajectories that begin at $\text{Re } x = +\infty$ and at $\text{Re } x = -\infty$.

We can perform the following asymptotic analysis valid near the pole at $x = i$: Let $x(t) = 1 + \epsilon(t)$. Then the equation of motion becomes approximately

$$[\epsilon'(t)]^2 \sim -2/\epsilon(t).$$

When we integrate this equation and assume that $\epsilon = 0$ at $t = 0$, we get

$$\epsilon(t) \sim 3^{2/3} 2^{-1/3} t^{2/3} e^{i\theta},$$

where $\theta = \pm \frac{\pi}{3}, \pi$. Thus, near the pole the separatrix splits into three lines separated by 120° . (This kind of

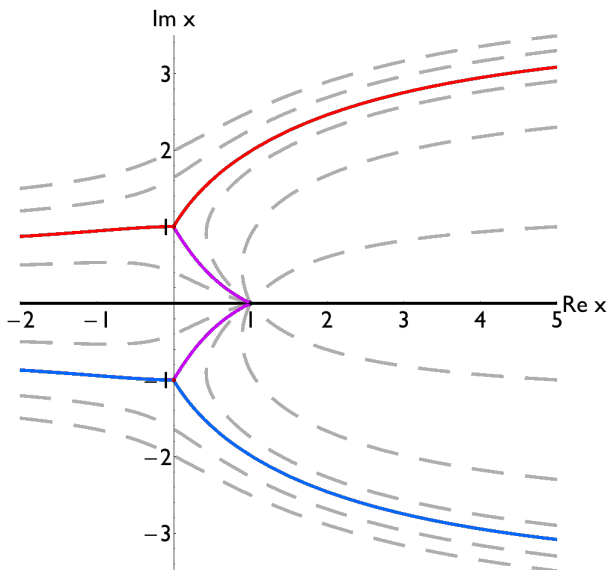


FIG. 8: Complex classical trajectories for the potential $V_1(x)$ in (11). The energy is $E = \frac{1}{2}$, so there is just one turning point at $x = 1$ and two poles at $x = \pm i$. Twelve trajectories (dashed lines) and separatrices (solid lines) are shown. A separatrix emerges from $x = i$ at 60° , -60° , and 180° . Trajectories start at $\text{Re } x = -2$, and $\text{Im } x = 0, \pm\frac{1}{2}$, and $\pm\frac{3}{2}$. Trajectories also start at $\text{Re } x = 5$ and $\text{Im } x = \pm 3.3, \pm 2.9, \pm 2.3, \pm 1$, and 0 . Three branches of the separatrix curve are shown in both the upper-half and the lower-half plane. The separatrices intersect at 120° angles at the poles. The separatrices end at the Zeno point (the turning point) $x = 1$, and they leave the plot at $x = -2 \pm 0.87i$ and at $x = 5 \pm 3.08i$.

behavior is reminiscent of the Stokes structure of Airy functions.) These features are shown in Fig. 8.

To perform an asymptotic study for large t we argue as follows. Since $x'(t) = \partial H / \partial p = 2p$, we get

$$\frac{1}{4}[x'(t)]^2 + \frac{x}{1+x^2} = \frac{1}{2}.$$

Therefore,

$$\int dx \frac{\sqrt{1+x^2}}{x-1} = t\sqrt{2} + C,$$

where C is a constant to be determined by the initial conditions. An exact evaluation of the integral gives

$$\sqrt{1+x^2} + \sqrt{2} \log \frac{x-1}{x+1+\sqrt{2+2x^2}} + \log \left(x + \sqrt{1+x^2} \right) = t\sqrt{2} + C. \quad (12)$$

To leading order $x \sim t\sqrt{2}$ as $t \rightarrow \infty$. However, a higher-order asymptotic approximation is

$$x \sim t\sqrt{2} - \log t + \sqrt{2} \log(1 + \sqrt{2}) - \frac{3}{2} \log 2 + K,$$

where

$$K = \sqrt{1+x_0^2} + \sqrt{2} \log \frac{x_0-1}{x_0+1+\sqrt{2+2x_0^2}} + \log \left(x_0 + \sqrt{1+x_0^2} \right). \quad (13)$$

We have performed a numerical calculation of the complex value of x on the separatrix at $t = 500$ and we have compared this result with the asymptotic analysis above. At $t = 500$ and for $x_0 = 1.1i$ we get

$$x_{\text{asymptotic}} = 701.113 + 3.8073i,$$

while

$$x_{\text{numerical}} = 701.124 + 3.8018i.$$

Evidently, the asymptotic analysis is highly accurate.

B. Phase transition behavior for $V_2(x)$

The potential $V_2(x)$ in (11) is \mathcal{PT} -symmetric. Consequently, the complex trajectories are left-right symmetric [1]. They start on the real axis or in the complex plane to the right of the imaginary axis and extend to mirror-image points to the left of the imaginary axis. We have studied the complex dynamical system described by the Hamiltonian $H = p^2 + V_2(x)$ and we have chosen the energy of the particle to be $E = 1$. Two turning points are located on the imaginary axis at $\frac{1}{2}(1 \pm \sqrt{5})i$ and two poles are located on the imaginary axis at $\pm i$. In summary, on the imaginary axis starting from below, there is a pole at $-i$, a turning point at $-0.618i$, a pole at i , and a turning point at $1.618i$. (See Fig. 9.)

We have calculated the transit time numerically from a point in the right-half plane to its mirror image in the left-half plane. There is a discontinuous (first-order) transition in this transit time. Below the separatrix curves the time is shorter than above. This discrete jump is due to the particle going just below or just above the poles at $\pm i$. The time differences of paths near the upper separatrix are illustrated in Fig. 10.

To understand the discontinuous curve in Fig. 10, note that below the pole at i the particle smoothly travels from an initial point on the positive real axis to its mirror point on the negative real axis. (The trajectory does not stop there.) The trajectory curves downward in response to the lower turning point. The high point of the trajectory passes just below the pole at i (and is horizontal there) but the trajectory is unaffected by the turning point. Rather, its gentle curvature is due to the more distant lower turning point at $-0.618i$. The pole at i screens the turning effect of the upper turning point. However, above the separatrix the trajectory passes just above and is strongly attracted by the upper turning point. So, the trajectory veers steeply upward, makes a sharp U-turn around the turning point, and goes downwards in a mirror-symmetric fashion.

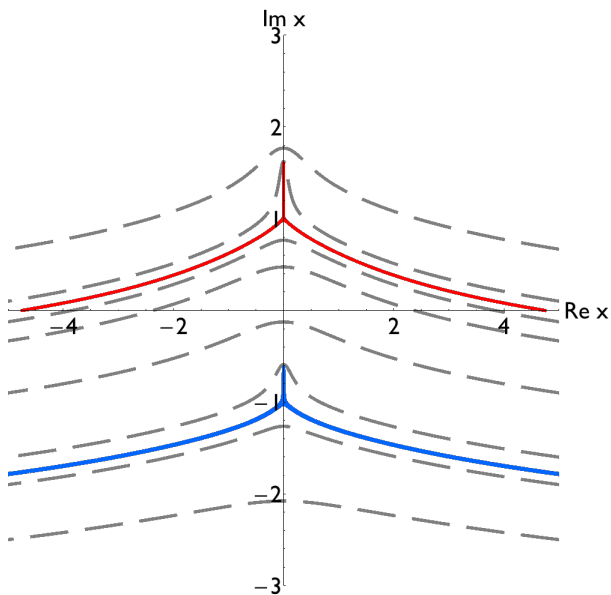


FIG. 9: Complex trajectories (dashed lines) of a classical particle of energy $E = 1$ in the potential $V_2(x)$. Four paths start at $5 + \frac{2i}{3}$ and $5 + \frac{i}{10}$ just above, and at $5 - \frac{i}{8}$ and $5 - \frac{i}{3}$ just below the upper separatrix (solid line), which starts on the real axis at 4.735 ± 0.005 . Four more paths begin at $5 - \frac{9i}{10}$, $5 - \frac{8}{5i}$ just above, and $5 - \frac{19i}{10}$ and $5 - \frac{5i}{2}$ just below the lower separatrix (solid line), which starts at $5 - 1.785 \pm 0.005i$. The poles are at $\pm i$ and the turning points are at $\frac{1}{2}(1 \pm \sqrt{5})i$. Trajectories below the lower separatrix are hardly affected by the turning points. Trajectories between the separatrices feel the effect of the lower but not the upper turning point. Trajectories above the upper separatrix only feel the effect of the upper turning point. Thus, trajectories just above a separatrix have a longer travel time than those just below a separatrix.

At the separatrix bifurcation the trajectory goes exactly up the imaginary axis from i to $\frac{1}{2}(1 + \sqrt{5})i = i\phi = 1.618i$ and back down to i . Using Hamilton's equation $\dot{x}(t) = \frac{\partial H}{\partial p} = 2p$, we find that the time T to do this is

$$\begin{aligned}
 T &= 2 \int_{x=i}^{i\phi} dt = 2 \int_{x=i}^{i\phi} \frac{dx}{\dot{x}(t)} \\
 &= \int_{x=i}^{i\phi} \frac{dx}{\sqrt{1 - ix/(x^2 + 1)}} \\
 &= 2 \int_{s=1}^{\phi} ds \sqrt{\frac{s^2 - 1}{1 + s - s^2}} \\
 &= 1.05659994.
 \end{aligned} \tag{14}$$

While Fig. 10 plots the transit time for a trajectory beginning and ending on the real axis, Fig. 11 extends these numerical results into the complex plane. In the positive quadrant each complex pixel x satisfying $0 \leq \text{Re } x \leq 5$ and $0 \leq \text{Im } x \leq 5$ is studied. The transit time is calculated and a color is assigned to indicate the transit time. The phase transition appears as the boundary curve sloping downward to the right.

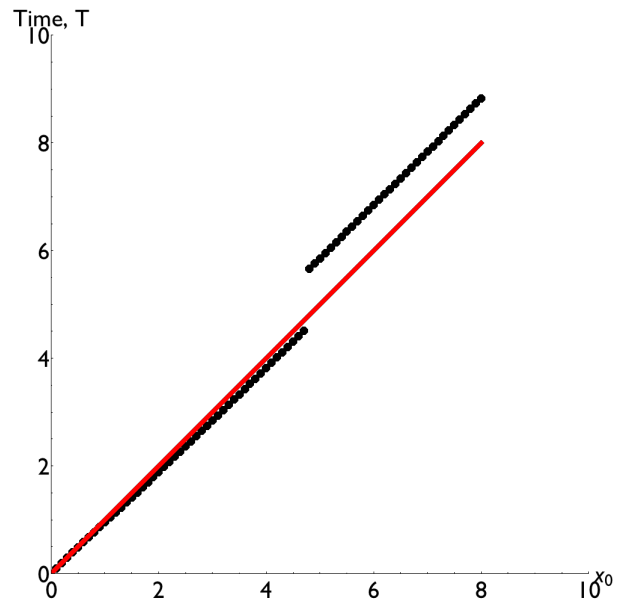


FIG. 10: Transit time for a particle of energy $E = 1$ to go from an initial point x_0 on the positive- x axis to its mirror-image point $-x_0$ on the negative- x axis. The solid line (red in electronic version) shows the transit time for a *free* particle of energy $E = 1$ to travel in the potential $V(x) = 0$. The dotted line (black in electronic version) is the transit time in the potential $V_2(x)$. The discontinuity is due to the particle going either below or above the pole at i . In the latter case the particle is pulled up and around the turning point at $1.618i$. In the former case the pole screens the trajectory of the particle from the effect of the turning point.

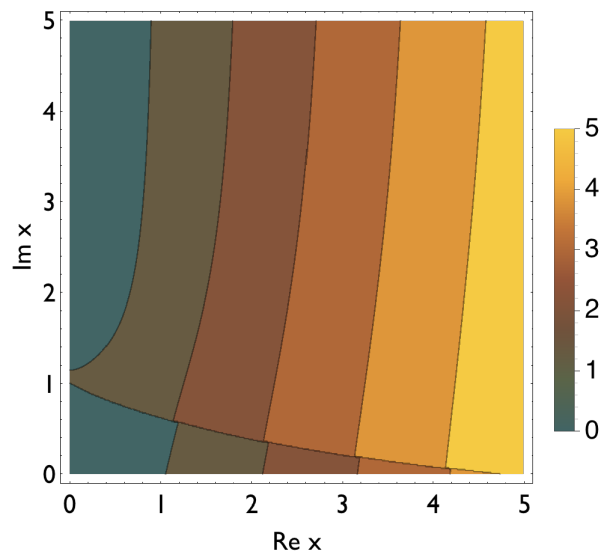


FIG. 11: Contour plot generalizing Fig. 10 from the real axis into the complex plane.

IV. TRAJECTORIES FOR $H = p^3 + V_1(x)$

Complex trajectories for Hamiltonians having higher powers of p have a rich and elaborate structure. Some previous studies were done in Ref. [11] but these studies focused on pairs of isospectral trajectories having identical periods. The current paper presents two results concerning Zeno behavior and bifurcation for the system described by the Hamiltonian $H = p^3 + V_1(x)$.

Recall from Sec. I that the phase space for such a p^3 Hamiltonian is very different from that of a p^2 Hamiltonian. The latter case is symmetric under classical time reversal $t \rightarrow -t$ and any point on a classical particle trajectory in the complex- x plane is associated with two values of \dot{x} pointing in opposing directions. One value corresponds to the forward time direction and the other to the backward time direction. However, in a p^3 model each point on a complex trajectory is associated with three velocities oriented at 120° to each other, and the correspondence with forward time evolution and backward time evolution is lost.

Figure 12 displays 18 trajectories (dashed lines) for a complex classical particle of energy $E = \frac{1}{2}$ governed by the Hamiltonian $H = p^3 + V_1(x)$. There are two poles on the imaginary- x axis at $x = \pm i$. A double turning point is situated at $x = 1$. Note that the structure of the trajectories is reminiscent of those shown in Fig. 8. The separatrix paths (solid lines) are now bent around to create what appears to be an enclosed area in the lower-half plane between the turning point and the lower pole. The turning point rotates classical particle trajectories in a manner that is more extreme than in a p^2 theory.

Figure 13 displays the trajectories for the same Hamiltonian that was used to generate Fig. 12, but now $E = \frac{1}{3}$. The trajectories in Fig. 13 are topologically complicated, so we have separated them into five components as shown in the five panels of Fig. 14. Figure 15 shows trajectories arising from different choices of initial velocities than those used in Fig. 13.

V. CONCLUDING REMARKS

We have examined Hamiltonians whose potentials have poles and zeros. We have seen that turning points attract trajectories while poles repel trajectories. We have also seen that trajectories in the complex- x plane can be extremely complicated for Hamiltonians in which the power of p is greater than 2, as shown in Figs. 13–15.

Things become even more interesting if the potential has an essential singularity, and such potentials should

be examined in future studies. For example, consider the potential $V(x) = e^{1/x}$, which has an essential singularity at the origin, and take the Hamiltonian $H = p^2 + V(x)$ and energy $E = e$. There is a turning point at $x = 1$ but there is also an infinite sequence of turning points at $x_n = r_n e^{i\theta_n}$, where r_n and θ_n satisfy the equations $\theta_n = \arctan(2n\pi)$ and $r_n = \cos(\theta_n)$. Thus, as $n \rightarrow \pm\infty$

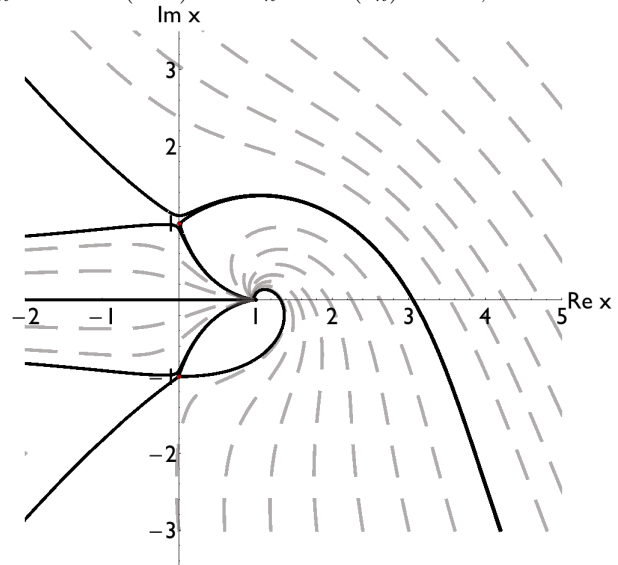


FIG. 12: Classical trajectories (dashed lines) for the Hamiltonian $H = p^3 + V_1(x)$ for particles of energy $E = \frac{1}{2}$. The behavior of trajectories near the pole at $x = i$ is emphasized. There are three branches of the separatrix curve (solid lines), which are separated by 120° .

there is an infinite sequence of turning points symmetrically placed above and below the origin with a limit point at the origin near $\pm\frac{\pi}{2}$. For $n = 1$ the turning point x_1 lies at $r_1 = 0.157177$ and $\theta_1 = 1.412965$ (an angle of 80.9569°). Figure 16 displays some complex classical trajectories for this potential. This figure shows that the essential singularity is attractive for trajectories approaching the essential singularity from the right and is repulsive for trajectories approaching from the left. Trajectories making U-turns around the turning point at $x = 1$ are shown. Trajectories around the turning points $x_{\pm 1}$ are also shown, but not shown is the infinite sequence of U-turns lying between these trajectories and approaching the negative-real axis!

CMB thanks the U.S. Department of Energy for financial support. Mathematica 9 was used to produce the numerical calculations and plots in this paper.

[1] C. M. Bender, S. Boettcher, and P. N. Meisinger, *J. Math. Phys.* **40**, 2201 (1999).
 [2] A. Nanayakkara, *Czech. J. Phys.* **54**, 101 (2004).

[3] A. Nanayakkara, *J. Phys. A: Math. Gen.* **37**, 4321 (2004).
 [4] F. Calogero, D. Gomez-Ullate, P. M. Santini, and M. Sommacal, *J. Phys. A: Math. Gen.* **38**, 8873 (2005).

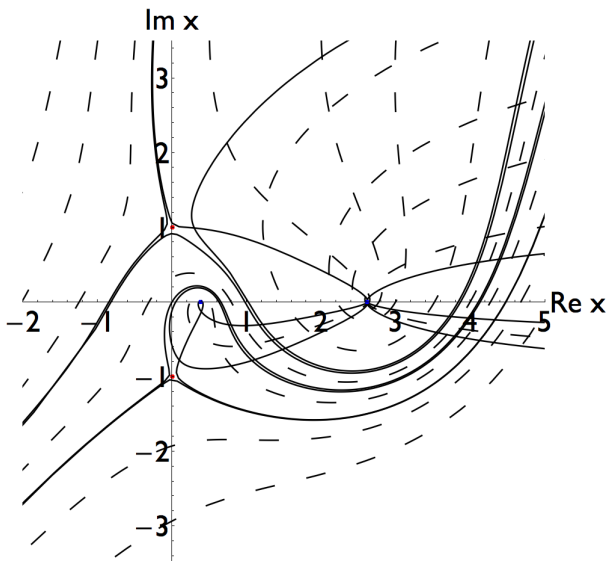


FIG. 13: Trajectories of a complex classical particle acting under the influence of the Hamiltonian $H = p^3 + V_1(x)$ (dashed lines). The energy of the particle is $E = \frac{1}{3}$. There are two poles at $x = \pm i$ and two turning points at $x = \frac{1}{2}(3 \pm \sqrt{5})$. This figure is analogous to Fig. 12 except that we have purposely chosen different directions for the velocities at the initial points. In the numerical analysis we have required that a path be smooth and not have elbows. Solid lines are separatrix paths that isolate different behaviors. Five different behaviors seen in this complicated figure are depicted separately in the five panels of Fig. 14.

- [5] C. M. Bender, J.-H. Chen, D. W. Darg, and K. A. Milton, *J. Phys. A: Math. Gen.* **39**, 4219 (2006).
- [6] Y. Goldfarb, I. Degani, and D. J. Tannor, *J. Chem. Phys.* **125**, 231103 (2006); Y. Goldfarb, and D. J. Tannor, *Ibid.* **127**, 161101 (2007).
- [7] C. M. Bender and D. W. Darg, *J. Math. Phys.* **48**, 042703 (2007).
- [8] C. M. Bender, D. D. Holm, and D. W. Hook, *J. Phys. A: Math. Theor.* **40**, F81 (2007)
- [9] C. M. Bender, D. D. Holm, and D. W. Hook, *J. Phys. A: Math. Theor.* **40**, F793 (2007).
- [10] Y. Fedorov and D. Gomez-Ullate, *Physica D* **227**, 120 (2007).
- [11] C. M. Bender and D. W. Hook, *J. Phys. A: Math. Theor.* **41**, 244005 (2008).
- [12] A. V. Smilga, *J. Phys. A: Math. Theor.* **42**, 095301 (2009).
- [13] C. M. Bender, D. C. Brody, and D. W. Hook, *J. Phys. A: Math. Theor.* **41**, 352003 (2008).
- [14] Y. Goldfarb, J. Schiff, and D. J. Tannor, *J. Chem. Phys.* **128**, 164114 (2008).
- [15] C. M. Bender and T. Arpornthip, *Pramana J. Phys.* **73**, 259 (2009).
- [16] C. M. Bender, J. Feinberg, D. W. Hook, and D. J. Weir, *Pramana J. Phys.* **73**, 453 (2009).
- [17] C. M. Bender, D. W. Hook, and K. S. Kooner, *J. Phys. A: Math. Theor.* **43**, 165201 (2010).
- [18] C. M. Bender, D. W. Hook, P. N. Meisinger, and Q. H. Wang, *Phys. Rev. Lett.* **104**, 061601 (2010) and *Ann. Phys.* **325**, 2332 (2010).
- [19] A. G. Anderson, C. M. Bender, and U. I. Morone, *Phys. Lett. A* **375**, 3399 (2011).
- [20] A. Cavaglia, A. Fring, and B. Bagchi, *J. Phys. A: Math. Theor.* **44**, 325201 (2011).
- [21] D. C. Brody and E.-M. Graefe, *J. Phys. A: Math. Theor.* **44**, (2011) 072001.
- [22] C. M. Bender and D. W. Hook, *J. Phys. A: Math. Theor.* **44**, 372001 (2011).
- [23] A. G. Anderson and C. M. Bender, *J. Phys. A: Math. Theor.* **45**, 455101 (2012).
- [24] C. M. Bender, D. W. Hook, and S. P. Klevansky, *J. Phys. A: Math. Theor.* **45**, 444003 (2012).
- [25] C. M. Bender and D. W. Hook, *Phys. Rev. A* **86**, 022113 (2012).
- [26] N. Turok, arXiv: quant-ph/1312.1771.
- [27] C. M. Bender and S. Boettcher, *Phys. Rev. Lett.* **80**, 5243 (1998).
- [28] P. E. Dorey, C. Dunning, and R. Tateo, *J. Phys. A: Math. Gen.* **34**, L391 (2001) and **34**, 5679 (2001).
- [29] P. E. Dorey, C. Dunning, and R. Tateo, *J. Phys. A: Math. Gen.* **40**, R205 (2007).
- [30] H. F. Jones and J. Mateo, *Phys. Rev. D* **73**, 085002 (2006).
- [31] C. M. Bender, D. C. Brody, J.-H. Chen, H. F. Jones, K. A. Milton, and M. C. Ogilvie, *Phys. Rev. D* **74**, 025016 (2006).

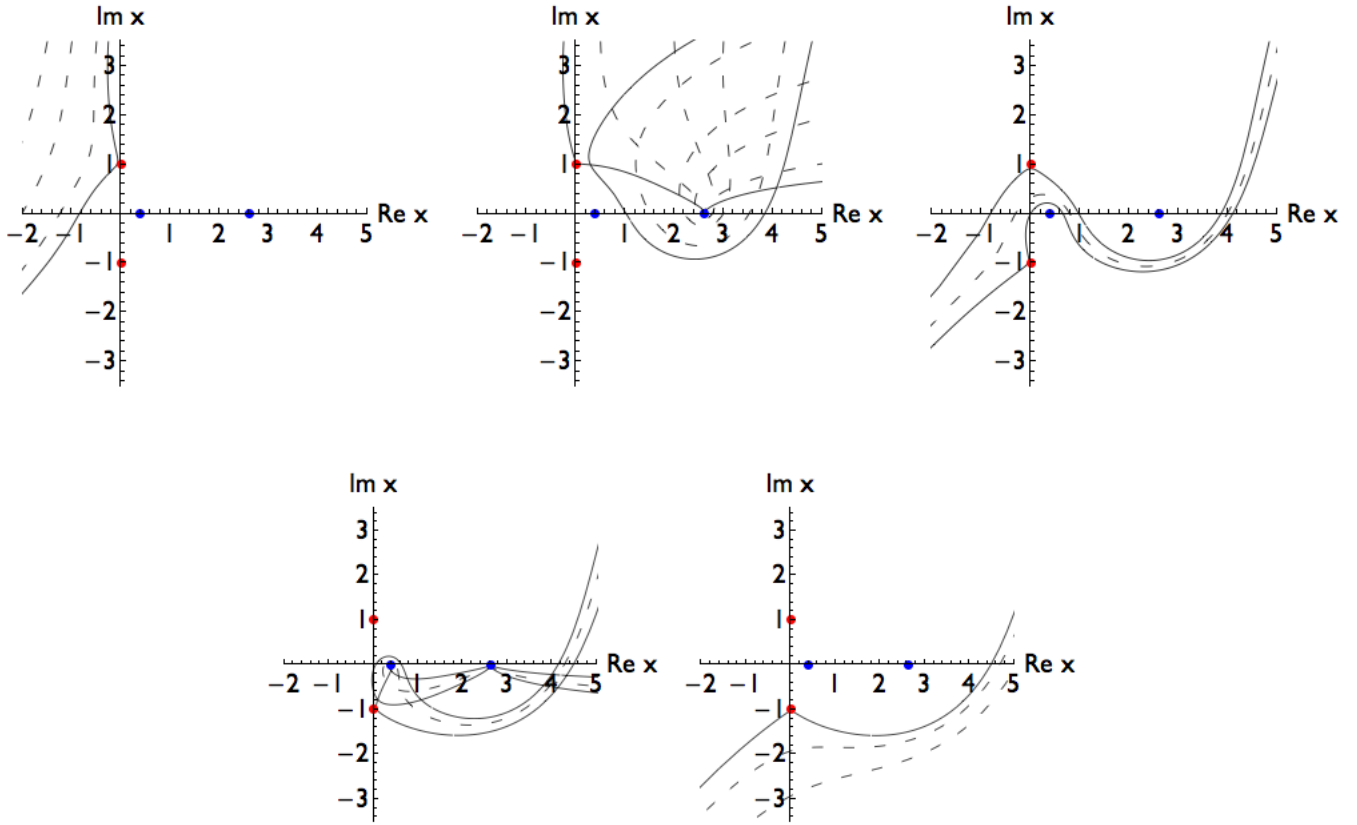


FIG. 14: Same as Fig. 13 but trajectories (dashed lines) are decomposed into regions between separatrices (solid lines). First panel on top row: All trajectories originate in the north and travel downward. The poles completely screen the trajectories from the turning points on the real- x axis. Middle panel on top row: All trajectories originate in the north and travel downward while under the control of the right turning point. Each trajectory turns through an angle of 240° onto a different sheet of the Riemann surface from that on which it entered the plot, and leaves the plot toward the east. Right panel on top row: A single trajectory shown between the two separatrix paths. The trajectory is turned by the right turning point but does not encircle it. Instead it comes under the control of the left turning point but does not encircle it either as it is repelled by the pole on the negative imaginary axis. Lower left panel: A trajectory starts in the northeast of the plot and goes in a downward direction. It is turned by the right turning point but is not close enough to encircle the turning point. It is then deflected by the pole at $x = -i$ and comes under the control of the left turning point, which it encircles. The trajectory then emerges from the left turning point on a different sheet of the Riemann surface and is instantly controlled by the right turning point, which it also encircles. The trajectory emerges from the right turning point on yet another Riemann sheet and exits the plot in an eastward direction. Bottom right panel: Two trajectories start on the right, are partially controlled by both turning points but are deflected by the pole before being captured, and instead exit the plot to the southwest.

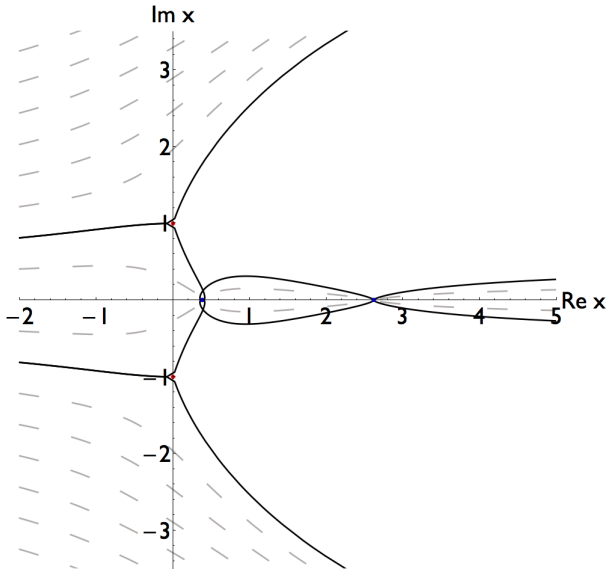


FIG. 15: As in Figs 13 and 14 but for a different set of initial conditions for the separatrix curves (solid lines). The trajectories have been chosen to be consistent with the initial directions of the separatrix curves.

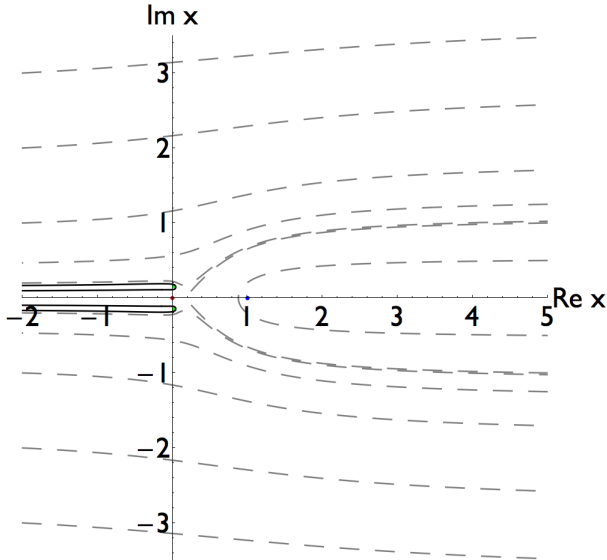


FIG. 16: Complex classical trajectories for the Hamiltonian $H = p^2 + V(x)$, where $V(x) = e^{1/x}$ and $E = e$. There is a turning point at $x = 1$. Note that the essential singularity at $x = 0$ is *both* attractive and repulsive depending on whether the particle approaches the origin from right-half or the left-half plane. There is one turning point at $x = 1$ and an infinite sequence of complex turning points x_n approaching the origin at $\arg x_n \rightarrow \pm \frac{\pi}{2}$ as $|n| \rightarrow \infty$.